

High Performance Pseudocapacitor Electrode Material Fabricated by Pulse Electro-Synthesized Cobalt Oxide Nanostructures

Mustafa Aghazadeh¹, Amir Rashidi¹, Parviz Norouzi^{2,3,*} and Mohammad Ghannadi Maragheh¹

¹ NFCRS, Nuclear Science and Technology Research Institute (NSTRI), P.O. Box 14395-834, Tehran, Iran

² Center of Excellence in Electrochemistry, University of Tehran, Tehran, Iran

³ Biosensor Research Center, Endocrinology and Metabolism Molecular-Cellular Sciences Institute, Tehran University of Medical Sciences, Tehran, Iran.

*E-mail: norouzi@khayam.ut.ac.ir

Received: 29 August 2016 / Accepted: 23 October 2016 / Published: 10 November 2016

High surface Co_3O_4 nanosheets were prepared were synthesized by a facile two-step approach, including a pulsed cathodic deposition without any surfactant and followed calcination of precursor. The as-deposited material was composed of pure β -cobalt hydroxide with sheet-like morphology. The calcined product was cubic spinel Co_3O_4 phase with sheet texture according to X-ray diffraction and scanning electron microscopy. The oxide formation on heating was discussed based on the thermogravimetric data. Brunauer-Emmett-Teller (BET) measurement showed the high surface area of about $164 \text{ m}^2 \text{ g}^{-1}$ for the prepared cobalt oxide nanosheets. The pseudocapacitor capacitance of the prepared electrode was as high as 501.6 F g^{-1} at a current density of 2 A g^{-1} , and the cycling stability remained about 89.9% after 2000 cycles. The fabricated electrode delivered energy and power densities of 29.43 Wh/Kg and 0.33 W/g , respectively. These results confirmed the high pseudocapacitive performance of the prepared active nanomaterials.

Keywords: Co_3O_4 ; Nanoplates; Pulse Electrodeposition; Heat-treatment; Supercapacitive performance

1. INTRODUCTION

Supercapacitors have received great attention because of their excellent storage performances including rapid charge/discharge ability, high power density and long cycle life [1-9]. Supercapacitors generally fall into two categories i.e. called electrical double-layer capacitors (EDLCs) and pseudocapacitors according to the specific energy storage mechanism. EDLCs store charge by the pure

electrostatic adsorption at the electrode-electrolyte interface [3], where the pseudocapacitors store energy through fast and reversible Faradic redox reactions and provide higher supercapacitive abilities [2,4]. Metal oxides/hydroxides such as RuO_2 [10], Ni(OH)_2 [11,12], Fe_3O_4 [13], Co(OH)_2 [14,15], V_2O_5 [16], Co_3O_4 [17,18], CeO_2 [19], MnO_2 [20-25] and NiO [26,27] can deliver higher specific capacitance (SC) than conventional carbon materials and better cycle life than polymer materials, because of the faradic charge-storage ability. Among these materials, spinel Co_3O_4 has high theoretical SC of 3560 F/g, a variety of oxidation states for efficient redox charge transfer, low cost and environmentally friendly [28]. Hence, many researches have been devoted to fabrication of novel high performance supercapacitor electrode based on the nanostructured Co_3O_4 with enhanced SC values and cycle life.

Up now, a variety preparation routes including thermal decomposition [29,30], chemical bath deposition [31,32], solvothermal [33,34], low-temperature oxidation [35], hydrothermal [18,36,37], and electrochemical synthesis [17,38-40] have been applied for the preparation of the nanostructured Co_3O_4 . As an electrochemical procedure, cathodic electrodeposition followed by annealing process has proven as an effective and facile technique for the preparation of nanostructured metal oxides with high electrochemical performances [41-45]. Hence, this method can be powerful technique for the preparation of nanostructured Co_3O_4 with enhanced charge storage ability. In the cathodic electrodeposition step, the cobalt hydroxide precursor is deposited on the cathode surface *via* base (OH^-) electrogeneration. The reports have shown that the uniform morphologies of the hydroxide precursor can be prepared by manipulating the applied electrochemical parameters [46-49]. The prepared deposited can be then calcined to obtain final nanostructured oxide. In this work, we applied pulse current in the electrodeposition of hydroxide precursor, and found that the pure $\beta\text{-Co(OH)}_2$ sheets is prepared as precursor. The hydroxide sheets are then calcined at 500 °C for 3h. The obtained analyses data from XRD, IR, BET and SEM revealed that the prepared cobalt oxide has composed of spinel Co_3O_4 with high surface area sheet-like structure. The charge storage ability of the prepared oxide was studied by cyclic voltammetry (CV) and charge-discharge techniques. The results indicate that the prepared spinel oxide can deliver high pseudocapacitor performance with delivering the energy and power densities of 29.43Wh/Kg and 0.33 W/g, respectively.

2. EXPERIMENTAL SECTION

2.1. Synthesis of cobalt hydroxide

The hydroxide precursor was deposited electrochemically onto a stainless steel (316L, surface area 100 cm^2). The two graphite plate with surface area of 100 cm^2 were fixed on the plexiglass holder and used as anodes. Notably the steel sheet was centered between these two graphite anodes. The cobalt hydroxide was deposited at room temperature in an additive-free bath only containing 0.01mol/L $\text{Co(NO}_3)_2$ using a pulse current (PC) mode. The deposition experiments were done at a typical on-times and off-times ($t_{\text{on}}=5\text{s}$ and $t_{\text{off}}=10\text{s}$) with an average current density of 2 mA cm^{-2} ($I_a =$

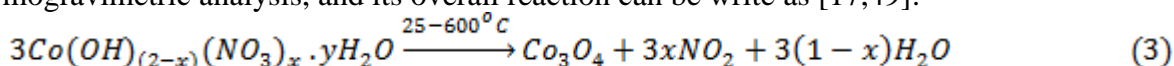
2 mA cm⁻²). The deposition time was 100 min. The cathodic reactions in the electrochemical deposition process are usually given as [47-49]:



After deposition, the steel sheet was brought out from the nitrate bath, washed several times with the deionized water and dried at RT for 48h. The deposit was scraped from the steel surface and the obtained brown powder was collected and named as hydroxide precursor.

2.2. Synthesis of cobalt oxide

The oxide sample was provided through the calcination of the hydroxide precursor prepared from electrodeposition procedure. In this way, the electrodeposited cobalt hydroxide powder was converted to cobalt oxide at 400 °C for 2h in dry air atmosphere. This conversion process was followed by thermogravimetric analysis, and its overall reaction can be write as [17,49]:



2.3. Characterization

Scanning electron microscopy was conducted using a LEO 1455VP scanning electron microscope (SEM) for surface morphology observation. The phase analyses of the prepared samples were performed by X-ray diffraction (XRD, Phillips PW-1800) using Cu K α radiation. FT-IR spectrum was obtained by a Bruker Vector 22 FT-IR spectrometer within the range of 400-4000 cm⁻¹ wave numbers. The measurement of specific surface area for the prepared oxide sample was performed through measuring N₂ adsorption-desorption isotherms at 77 K with a Quanta-chrome NOVA-2200e system. Cyclic voltammetry (CV) and galvanostatic charge-discharge (GCD) tests were performed by use of a potentiostat (AUTOLAB[®], Eco Chemie, PGSTAT 30). A three-electrode electrochemical cell containing; the fabricated Co₃O₄ paste as working electrode, Ag/AgCl (1 M KCl, saturated) as reference electrode, platinum wire as the counter electrode, and 1M KOH aqueous solution as electrolyte, was used for the CV and GCD tests. The working electrode was prepared by mixing the prepared nanostructured Co₃O₄, acetylene black, conducting graphite and polytetrafluoroethylene (PTFE) binder (with the weight ratios of 75:10:10:5, respectively). The prepared mixture was pressed under 10 MPa into steel mesh current collectors (1 cm × 1 cm) and then dried in oven for 10 min at 70 °C. The CVs were collected in a potential range between -0.1 and 0.55 V vs. Ag/AgCl at the scan rates of 2, 5, 10, 25, 50 and 100 mV s⁻¹. The GCD profiles were recorded at the current densities of 0.2, 0.5, 1, 2, 3, 5, 7 and 10 A g⁻¹ within a potential range of -0.1 to 0.5 V vs. Ag/AgCl. The SCs of the fabricated Co₃O₄ electrode were calculated from the CVs and GCD profiles using Eqs. (4) and (5);

$$C = \frac{1}{m\vartheta(V_a - V_c)} \int_{V_a}^{V_a} I(V) dV \quad (4)$$

where C is the SC of Co₃O₄ (F g⁻¹), V_a is the cut of value of anodic section, V_c is the cut of cathodic potential, m is the mass of Co₃O₄ used in the fabricated electrode (g), v is the scan rate (V s⁻¹)

and I(V) is a current response during the scan of potential. The mass loading of active materials was 2.2 mg.

$$C = \frac{I \times \Delta t}{m \times \Delta V} \tag{5}$$

where C is the calculated SC for Co₃O₄ electrode, I is the applied current load (A), ΔV is the potential window (0.65 V), Δt is the time of a discharge cycle (s) and m is the mass of Co₃O₄ (g).

3. RESULTS AND DISCUSSION

3.1. Thermogravimetric data

To obtain the oxide product, the prepared deposit was calcined at 400°C for 2h. The conversion of hydroxide to oxide was specified through DSC-TG analysis and the results are shown in Fig. 1.

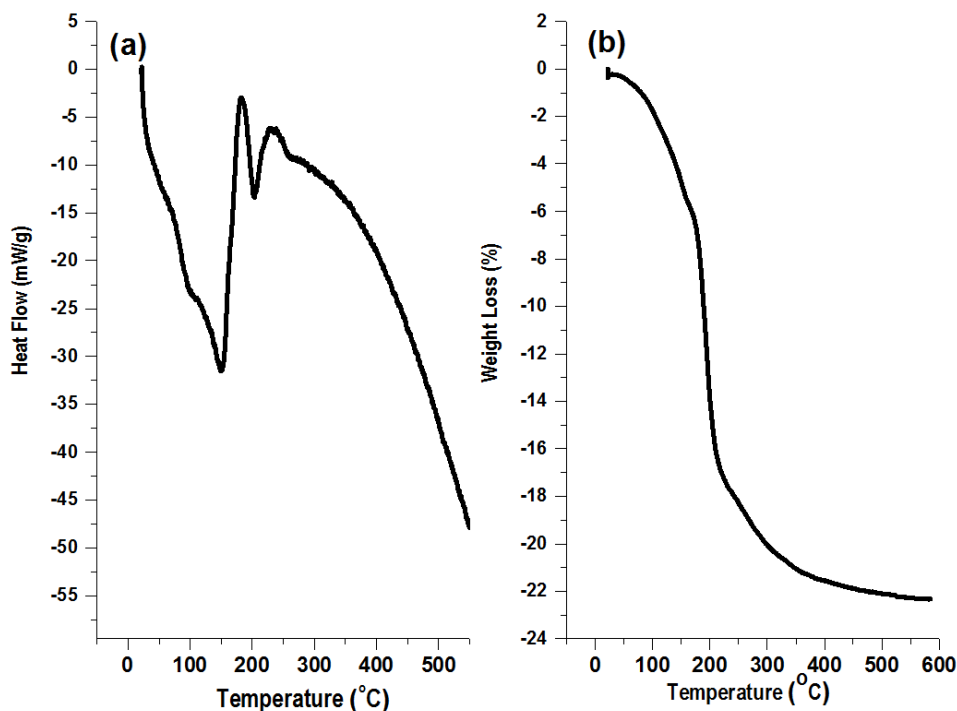
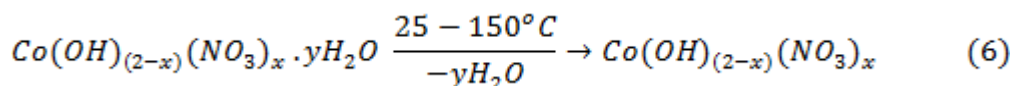
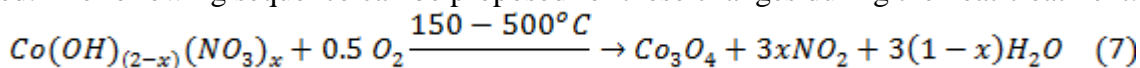


Figure 1. (a) DSC and (b) the related TG profiles for the deposited hydroxide sample.

The DSC profile of the hydroxide precursor (in Fig. 4a) has three continuous endothermic peaks at the temperature range of 25-300 °C. TG curve is exhibited total weight loss of 22.7% during heating. The first peak in the DSC curve is due to the removal of the water molecules adsorbed on the hydroxide deposit (Eq. 6). TG curve showed a 4.6 wt% weight loss for this step.



According to the endothermic peaks of DSC, the structural water is also removed at about 150-400°C, which is consistent with the reported data in Refs [33,36,38]. TG curve showed 17.3% weight loss for these changes. Notably, after this weight loss step, a small weight loss (0.8%) up to 500 °C. This last change is related to the removal of nitrate ions [46,49]. For this step, a small weight loss is observed. The following sequence can be proposed for these changes during the heat-treatment:



3.2. Structural characterization

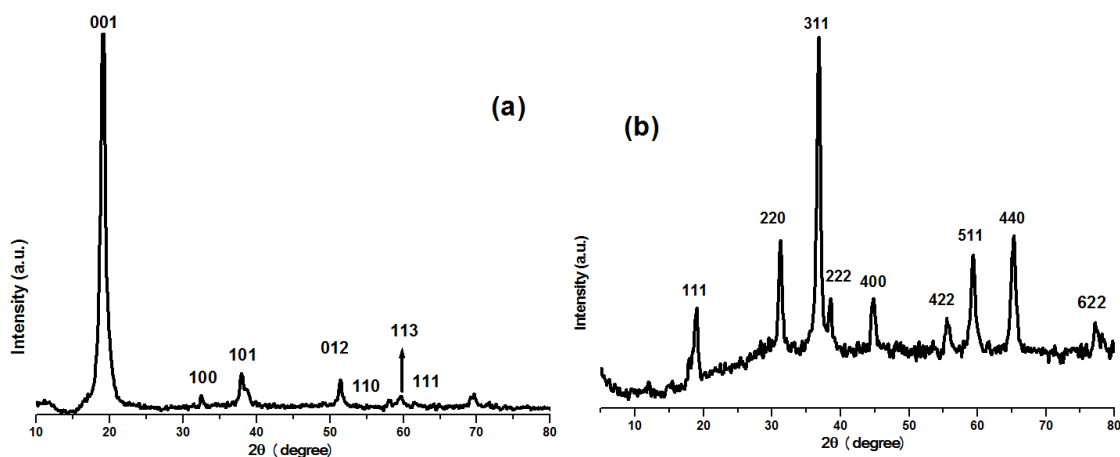


Figure 2. XRD patterns of (a) hydroxide and (b) oxide samples.

Fig. 2 presents XRD patterns of the hydroxide precursor and final oxide product. The XRD pattern of the deposited hydroxide precursor can be fully indexed to the hexagonal brucite-like structure of the β - $\text{Co}(\text{OH})_2$ phase (JCPDS file #74-1057). Notably, the (001) diffraction peak (at 11.5°) has high intensity as compared with other diffraction peaks of the deposited hydroxide. This implies the preferred orientation of the deposited hydroxide with the c-axis parallel to the substrate surface, as observed by SEM (Fig. 4). No other phase (i.e. alpha-cobalt hydroxide) peaks are observed, demonstrating that the deposited hydroxide has composed of pure β - $\text{Co}(\text{OH})_2$ phase. In Fig. 2b, the diffraction peaks observed at 19.4° , 32.1° , 36.9° , 44.2° , 59.1° , 65.1° and 78.3° is related to the (111), (220), (311), (400), (511), (440) and (622) reflections of Co_3O_4 , respectively. In fact, all the reflections can be indexed to the typical Co_3O_4 phase with lattice constant $a = 8.084 \text{ \AA}$ (space group $Fd3m$), and corresponding to the standard reference data of JCPDS file#42-1467. No any diffraction peak related to secondary or impurity phases were found, confirmed the high purity of the final products, and complete conversion of the hydroxide precursor to the cobalt oxide after calcination at 400°C for 2h.

The FTIR spectra of the prepared hydroxide and oxide samples are shown in Fig. 3. The IR spectra of the hydroxide sample has main bands related to the pure β - $\text{Co}(\text{OH})_2$ phase, as follow; (i) the narrow band at 3637 cm^{-1} is corresponds to the $\nu_{\text{O-H}}$ stretching of the OH groups in the brucite-like structure [48,49], (ii) the two main bands at low wave numbers of 665 cm^{-1} and 497 cm^{-1} are the $\delta_{\text{Co-O}}$.

δ_{H}) and $\gamma_{(\text{Co-O})}$, in the brucite-like octahedron, respectively, [17,50], (iii) the sharp bond at 1383 cm^{-1} is related to the nitrate stretching vibration, and confirmed the nitrate intercalation in the hydroxide deposit [11,47], (iv) the bonds at 3442 cm^{-1} and 1628 cm^{-1} are the hydroxyl group and water molecules vibrations, (v) the peaks at about 1476 , 1096 , and 847 cm^{-1} are attributed to the carbonate groups and also some of nitrate ions vibrations [13-15]. These IR data clearly confirmed the brucite-like structure (i.e. $\beta\text{-Co(OH)}_2$ phase) of the deposited hydroxide.

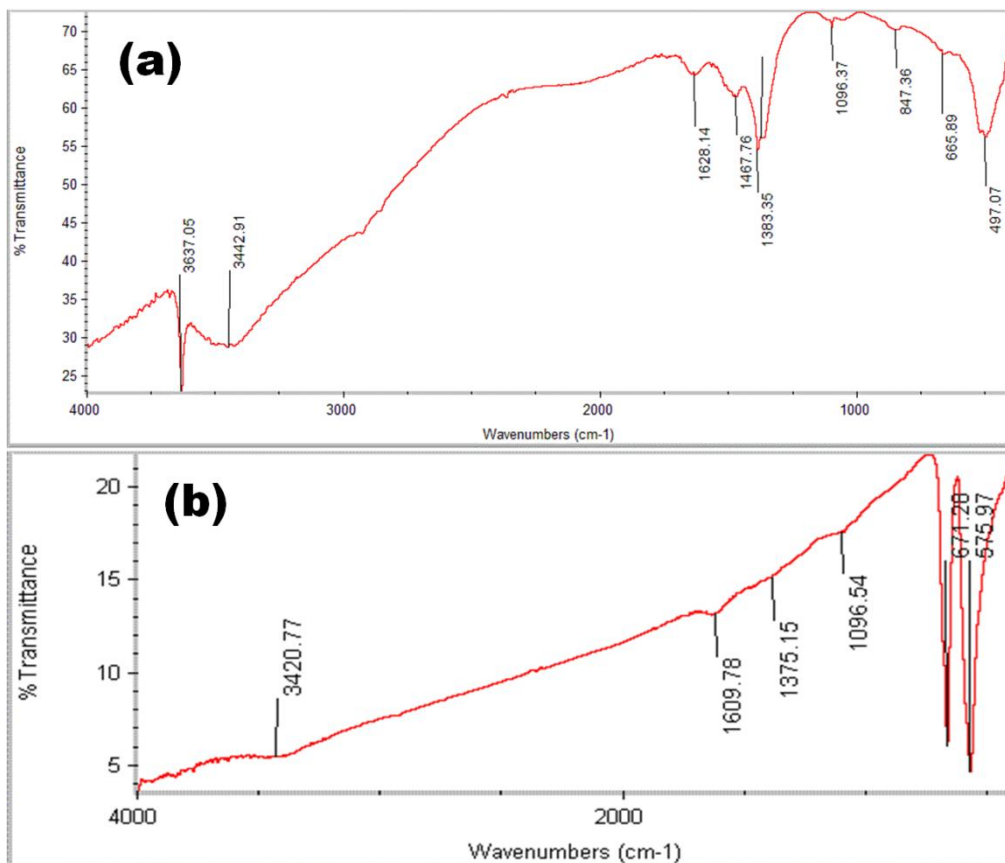


Figure 3. IR spectra of (a) hydroxide and (b) oxide samples.

The spectra in Fig. 3b is also has main IR bands of the spinel cobalt oxide. In this way, the bands at 671 cm^{-1} and 575 cm^{-1} are correspond to the OB_3 (B represents Co^{3+} in an octahedral hole) and the ABO (A represents the Co^{2+} in a tetrahedral hole) vibrations in the spinel lattice, respectively [17, 33, 37]. The two bands at 3420 cm^{-1} and 1609 cm^{-1} are associated with the stretching and bending vibrations of hydroxyl groups and H_2O molecules. The peaks located at about 1376 and 1096 cm^{-1} are attributed to the carbonate groups originating from the reaction of cobalt oxide with air- CO_2 during the IR analysis procedure.

The surface morphology of the prepared samples is shown in Fig. 4. For both prepared samples, a sheet-like texture can be clearly seen in the SEM images. There are some cavities/or pores between the sheets, may originates from the hydrogen bubbling on the cathode surface, as previously observed by Nguyen *et al.* [51]. These cavities can facilitate the electrolyte penetration into the active area and results the high contribution of active materials (i.e. oxide sheets) in the charge storage

performance. The observed sheets are not uniform hexagonal shape and some irregularity is seen, which may provide the high surface area of the prepared cobalt oxide. The surface area of the oxide product was measured using the Brunauer–Emmett–Teller (BET) method.

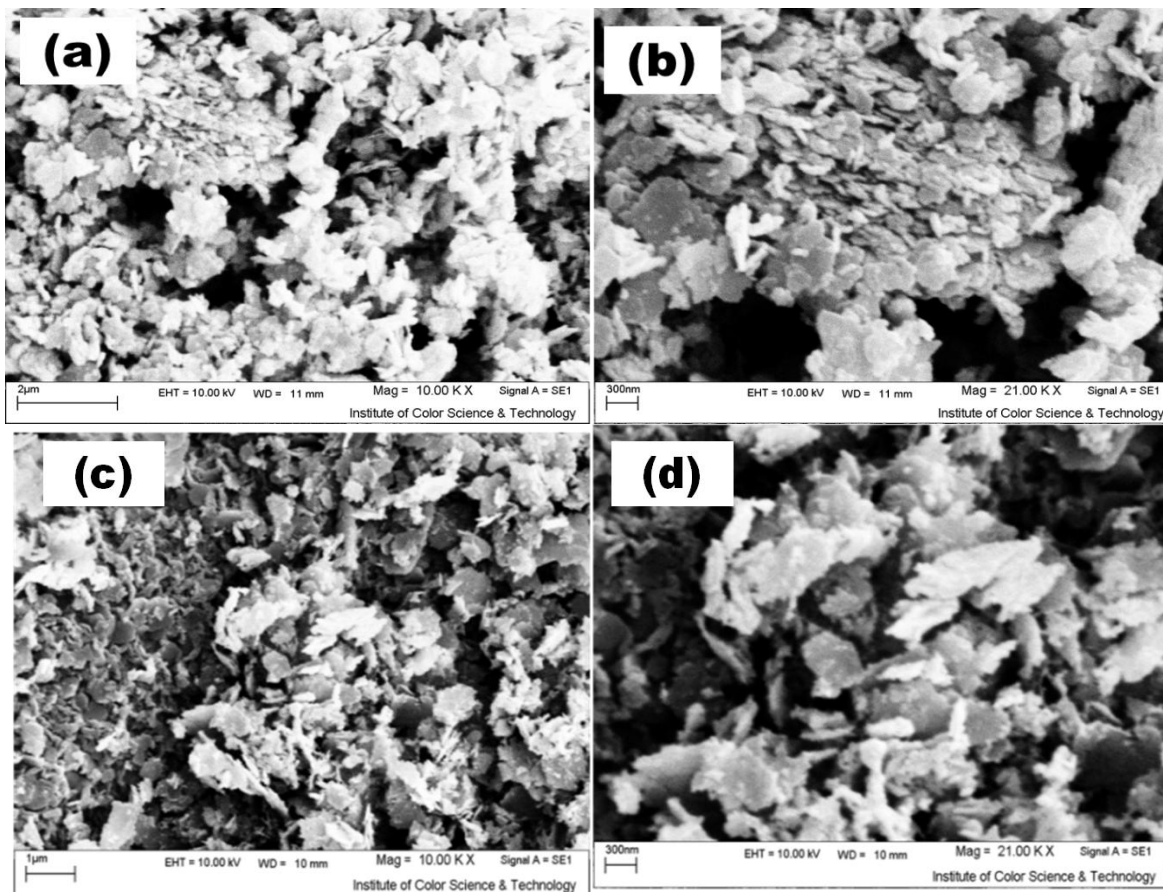


Figure 4. (a,b) SEM images of the deposited hydroxide and (c,d) SEM images of the oxide product.

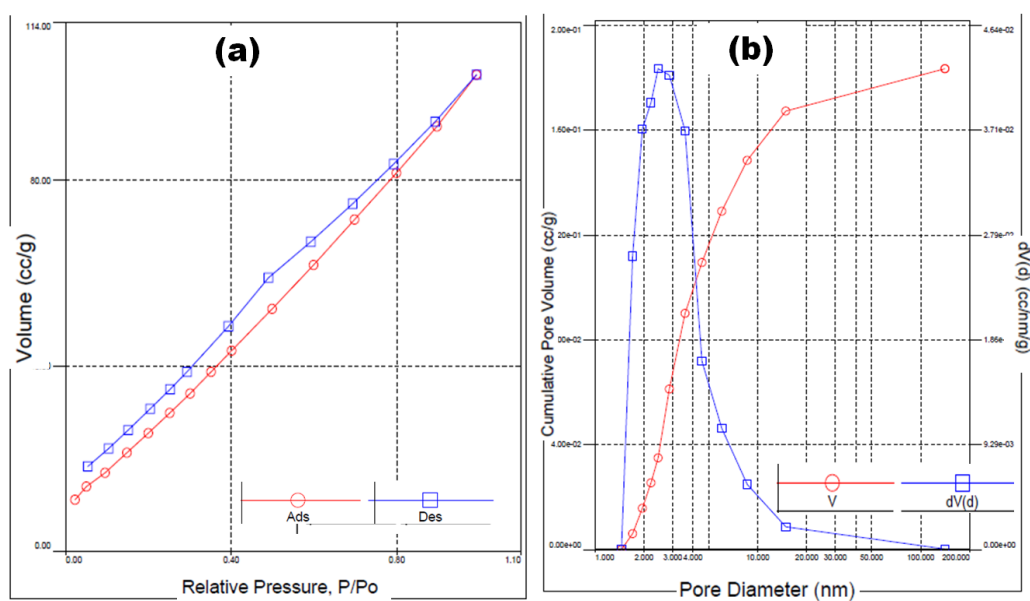


Figure 5. (a) BET and (b) BJH pore size distribution curves of Co₃O₄ nanosheets.

Fig. 5 shows the surface area measurement and pore size distribution of the prepared Co_3O_4 nanosheets. The N_2 isotherm of the prepared oxide has a type II form with a large type H4 hysteresis loop, which implies the existence of micro-porous materials according to the IUPAC classification [52]. The Co_3O_4 nanosheets have a high BET surface area of $164 \text{ m}^2 \text{ g}^{-1}$. The pore size distribution profile is exhibited in Fig. 5b. It can be seen that the oxide texture has pores with size 2-4 nm. This range of pore size may provide good electrolyte penetration and its access during the charge-discharge test. Also, its expected that stable conditions provided for the hydroxyl ions insertion/deinsertion during the charge/discharge cycling, where the improved cycle life be observed for the fabricated electrode. Hence, its expected that the prepared sample deliver high supercapacitive performance.

3.3. Supercapacitive performance

Cyclic voltammetry (CV) and galvanostat charge-discharge (GSD) tests were used to evaluate the supercapacitive performance and quantify the SCs of the fabricated Co_3O_4 electrode. It was reported that Co_3O_4 capacitor in an alkaline solution exhibits both types of charge storage mechanisms [37,38,53] i.e. the electric double layer behavior at the electrode–electrolyte interface and faradic redox charge storage at the host material through hydroxyl ion diffusion.

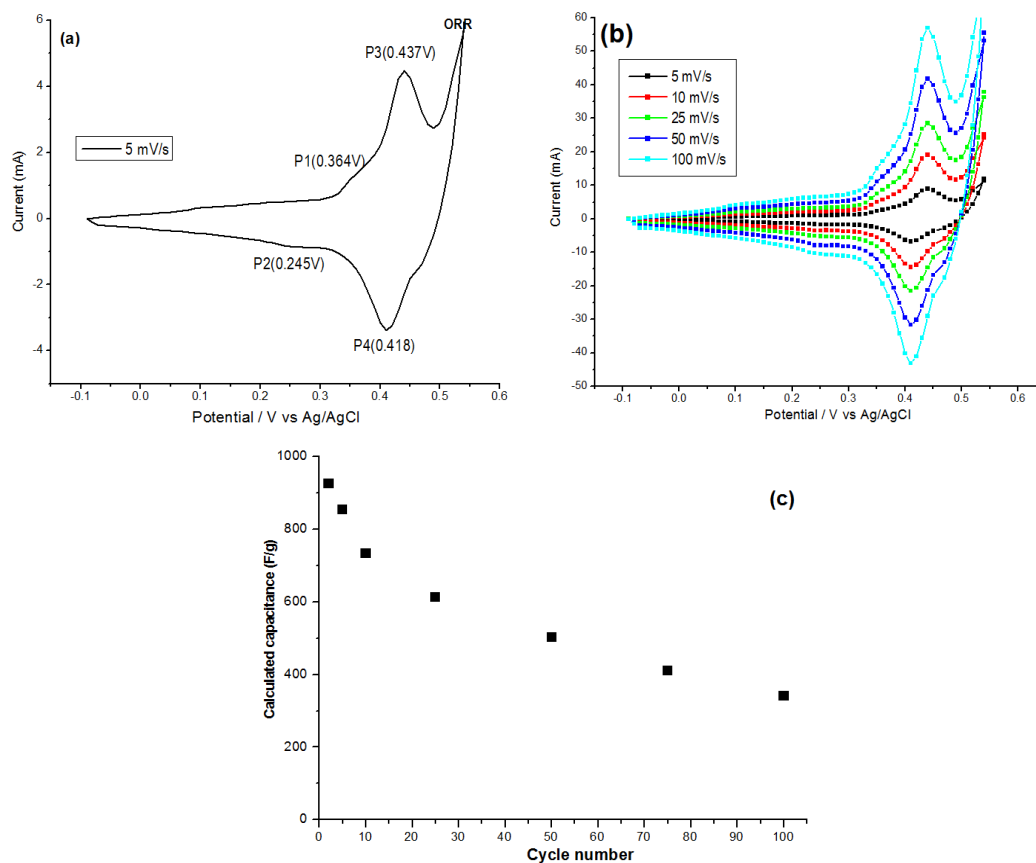


Figure 6. (a) CVs of Co_3O_4 electrode at 5 mV/s and (b) at the various scan rates, (c) the calculated SCs vs. scan rate.

Fig. 6 shows the CVs of the prepared Co₃O₄ electrode at the different scan rates and the calculated capacitances at each scan rate. The potential range was from -0.1 to 0.55 V (vs. Ag/AgCl) in 1 M KOH aqueous solution. The workable potential range for our prepared electrode is higher than those of the Co₃O₄ nanostructure electrode reported in Refs [29-37,53]. Notably, the performance in the wide potential range is key factor in the supercapacitive evaluation of any electro-active material.

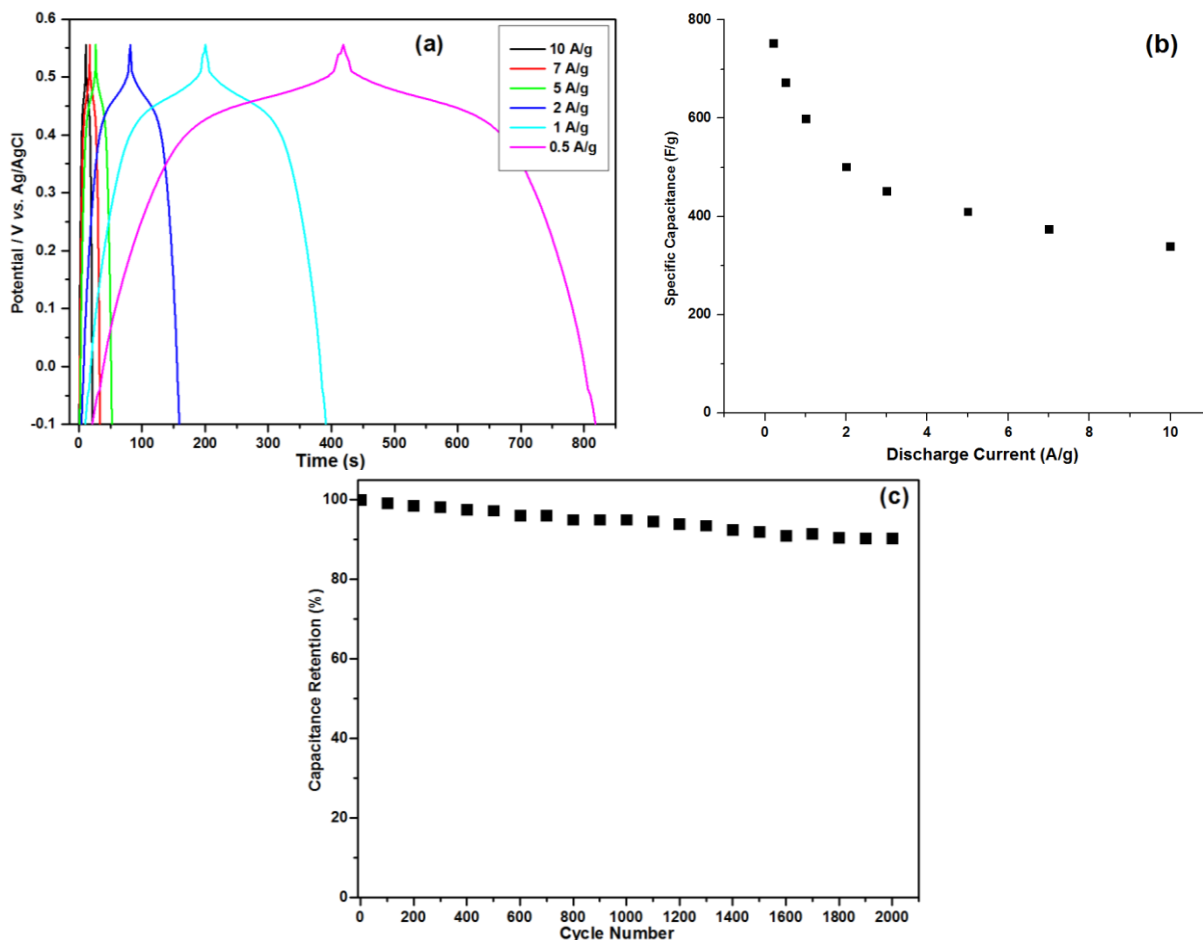
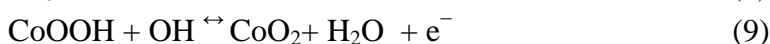


Figure 7. (a) the GCD profiles and (c) calculated SCs at the different current loads, (d) capacity retention for 3000 charge-discharge cycling at the current load of 2 A g⁻¹.

As can be seen from Fig. 6a, the Co₃O₄ electrode exhibits two pair redox peaks, indicating that the measured capacitances are mainly based on the redox mechanism. Furthermore, when increasing the scan rate, peak currents were also increased, indicating good reversibility of the fast charge-discharge response of the materials as seen in Fig. 6b. As illustrated in the CV curves, two pairs of redox peaks i.e. p₁/p₂ and p₃/p₄ appear, which are considered to arise from Co²⁺/Co³⁺ reaction and the conversion between Co³⁺ and Co⁴⁺, respectively [17,53]. These redox reactions of the prepared electrode can be expressed as follows [39,53]:



The average SCs of the prepared Co_3O_4 electrode were estimated from the CVs in Fig. 6b using Eq. (4) via integrating the area under I-V curves. Fig. 6c presents the calculated SCs at the different applied scan rates. It can be seen that the fabricated electrode is capable to deliver the SCs as high as 854.2, 728.8, 613.9, 501.8, 410 and 339.5 F g^{-1} at scan rates of 5, 10, 25, 50, 75 and 100 mV s^{-1} , respectively. The values showed excellent supercapacitive performance of the prepared sample, which special morphology and high surface area.

The GCD profiles were also recorded at the different current density of 0.2, 1, 2, 3, 5, 7 and 10 A g^{-1} which are shown in Fig. 7a. The SCs of the electrode at the applied current densities were then calculated via the Eq. (5), which is presented in Fig. 7c. The calculations resulted that the prepared cobalt oxide nanosheets are capable to deliver the SCs as high as 752.4, 672, 599.3, 501.6, 452.5, 410.8, 374.1 and 339.4 F g^{-1} at scan rates of 0.2, 0.5, 1, 2, 3, 5, 7 and 10 A g^{-1} , respectively (Fig. 7c). These values are in agreements with the calculated ones from the CVs (Fig. 6a) and also confirmed an excellent supercapacitive behavior for the Co_3O_4 nanosheets. Furthermore, the observed capacitances are comparable with the reported ones for nanostructured Co_3O_4 prepared by different synthesis methods until now [30-40]. To investigate the cycle life of the fabricated Co_3O_4 electrode, the GCD cycling (2000 cycles) in 1M KOH electrolyte was also recorded at the current load of 2 A g^{-1} . The SC of each cycle was calculated via Eq. (5) and, based on the obtained SCs, the capacity retention of the Co_3O_4 electrode on cycling was evaluated, as shown in Fig. 7c. The results showed that the prepared nanoplates have high stable capacitances during cycling where they exhibited excellent specific capacitance retention of ca. 89.9% after 2000 continuous cycling. These observations confirmed that the prepared Co_3O_4 nanosheets are excellent candidate for long-time capacitor performance in KOH. The coulombic efficiency (η) was also calculated from GCD tests as follow [38]:

$$\eta = (Q_d/Q_c) * 100 = (\Delta t_d/\Delta t_c) * 100 \quad (10)$$

Where Q_d and Q_c are the electric charge for discharging and charging steps, respectively. Δt_c and Δt_d are the times of charging and discharging, respectively. According to the Eq. (10), the η values were obtained to be about 99.9%, 95.5%, 92.1% and 89.5 % for the 10th, 500th, 1000th and 2000th cycle of GCD profile at the charge load of 2 A g^{-1} . The energy density (E) and power density (P) of the fabricated electrode were also calculated by the following equations [39,54]:

$$E (\text{Wh Kg}^{-1}) = 1/2 * C * (\Delta V)^2 * (1000/3600) \quad (11)$$

$$P (\text{kWh Kg}^{-1}) = E/t \quad (12)$$

Here, t and ΔV are the discharge time and the potential window of cycling, respectively. It was obtained that our electrode exhibits energy and power densities of 29.43Wh/Kg and 0.33 W/g, respectively. These data confirmed the high performance characters of the prepared nanomaterials.

4. CONCLUSION

We synthesized high surface area cobalt oxide with sheet-like morphology and evaluated their capacitor properties when they were used as electrode materials. By applying the pulse current mode into the two electrochemical cell and pulsed base electrogeneration on the cathode surface, the cobalt hydroxide precursor was effacingly prepared. The structural and morphological data revealed that the

deposited precursor has pure β phase of $\text{Co}(\text{OH})_2$ nanosheets. By calcination, this hydroxide sample was converted to the cobalt oxide, which was investigated through DSC-TG analysis. The electrochemical performance tests of oxide sample indicated that the Co_3O_4 sheets exhibited ultrahigh SC values of 752.4, 672, 599.3, 501.6, 452.5, 410.8, 374.1 and 339.4 F g^{-1} at scan rates of 0.2, 0.5, 1, 2, 3, 5, 7 and 10 A g^{-1} , respectively. After 2000 cycles, Co_3O_4 sheets high cycling reversibility and only slightly decayed less than 10% at a current density of 2 A/g .

ACKNOWLEDGEMENTS

Authors are grateful to the research council of University of Tehran for the financial support of this work.

References

1. Y. Wang, Y. Song, and Y. Xia, *Chem. Soc. Rev.* (2016) Advance Article DOI: 10.1039/C5CS00580A
2. H. Xiao, S. Yao, H. Liu, F. Qu, X. Zhang and X. Wu, *Progress in Natural Science: Mater. Int.* 26 (2016) 271.
3. P. Sharma, and T.S. Bhatti, *Energy Conversion and Management* 51 (2010) 2901.
4. H. Gholipour-Ranjbar, M. R. Ganjali, P. Norouzi and H. R. Naderi, *Mater. Res. Express* 3 (2016) 075501.
5. J. S. Shayeh, A. Ehsani, M. R. Ganjali, P. Norouzi, and B. Jaleh, *Applied Surface Science* 353 (2015) 594.
6. H. R. Naderi, P. Norouzi, M. R. Ganjali and H. Gholipour-Ranjbar, *Powder Technol.* 302 (2016) 298.
7. K. Adib, M. Rahimi-Nasrabadi, Z. Rezvani, S.M. Pourmortazavi, F Ahmadi, H. R. Naderi, and M. R. Ganjali, *J. Mater. Sci.* 27 (2016) 4541.
8. H. Gholipour-Ranjbar, M.R. Ganjali, P. Norouzi, and H.R. Naderi, *Ceram. Int.* 42 (2016) 12097.
9. H. R. Naderi, M. R. Ganjali, A. S. Dezfouli and P. Norouzi, *RSC Advances* 6 (2016) 51211.
10. T. P. Gujar, W.-Y.Kim, I. Puspitasari, K.-D.Jung, and O.S. Joo, *Int. J. Electrochem. Sci.*, 2 (2007) 666.
11. M. Aghazadeh, B. Sabour, M.R. Ganjali, and S. Dalvand, *Appl. Surf. Sci.* 313 (2014) 581.
12. J. Tizfahm, B. Safibonab, M. Aghazadeh, A.Majdabadi, B. Sabour, and S. Dalvand, *Colloids Surf.* A443 (2014) 544.
13. M. Jayalakshmi, and K. Balasubramanian, *Int. J. Electrochem. Sci.*, 4 (2009) 878.
14. J. Talat Mehrabad, M. Aghazadeh, M. Ghannadi Maragheh, M. R. Ganjali, and P. Norouzi, *Mater. Lett.* 184 (2016) 223.
15. M. Aghazadeh, A.-A. Malek Barmi, D. Gharailou, M. H. Peyrovi, B. Sabour, and F. Najafi, *Appl. Surf. Sci.* 283 (2013) 871.
16. D. Shu, C. Lv, F. Cheng, C.He, K. Yang, J. Nan, and L. Long, *Int. J. Electrochem. Sci.*, 8 (2013) 1209.
17. M. Aghazadeh, R. Ahmadi, D. Gharailou, M. R. Ganjali, and P. Norouzi, *J. Mater. Science: Mater. Electron.* 27 (2016) 8623.
18. Y. Liang, Y. Yang, Z. Hu, Y. Zhang, Z. Li, N. An, and H. Wu, *Int. J. Electrochem. Sci.*, 11 (2016) 4092.
19. N. Maheswari, and G. Muralidharan, *Energy & Fuels* 29 (2015) 8246.
20. H. Gholipour-Ranjbar, M. R. Ganjali, P. Norouzi and H. R. Naderi, *J. Mater. Sci.* 27 (2016) 10163.
21. H. R. Naderi, P. Norouzi and M. R. Ganjali, *Applied Surface Science* 366 (2016) 552.

22. J. Tizfahm, M. Aghazadeh, M. Ghannadi Maragheh, M.R. Ganjali, P. Norouzi, and F. Faridbod, *Mater. Lett.* 167 (2016) 153.
23. M. Aghazadeh, M. Asadi, M. Ghannadi Maragheh, M.R. Ganjali, P. Norouzi, and F. Faridbod, *Appl. Surf. Sci.* 364 (2016) 726.
24. H. R. Naderi, M. R. Ganjali, and P. Norouzi, *Int. J. Electrochem. Sci.* 11 (2016) 4267.
25. M. Aghazadeh, M. Ghannadi Maragheh, M.R. Ganjali, and P. Norouzi, *RSC Adv.* 6 (2016) 10442.
26. M. Aghazadeh, *J. Mater. Science: Mater. Electron.* (2016) in press.
27. A. Barani, M. Aghazadeh, M.R. Ganjali, B. Sabour, A.A. Malek Barmi, and S. Dalvand, *Mater. Sci. Semiconduct. Process* 23 (2014) 85.
28. K. K. Lee, W.S. Chin, and C.H. Sow, *J. Mater. Chem. A* 2 (2014) 17212.
29. Y. Yoon, and J. MyounKo, *Int. J. Electrochem. Sci.*, 3 (2008) 1340.
30. E. Laouini, M. Hamdani, M.I.S. Pereira, Y. Berghoute, J. Douch, M. H. Mendonça, and R.N. Singh, *Int. J. Electrochem. Sci.*, 4 (2009) 1074
31. S.U. Offiah, A.C. Nwanya, S.C. Ezugwu, B.T. Sone, R.U. Osuji, M. Malik, C.D. Lokhande, and F.I. Ezema, *Int. J. Electrochem. Sci.*, 9 (2014) 5837.
32. K. Deori, S. Kumar Ujjain, R. K. Sharma, and S. DeKa, *ACS Appl. Mater. Interfaces* 5 (2013) 10665.
33. F. Zhang, L.Hao, L. Zhang, and X. Zhang, *Int. J. Electrochem. Sci.*, 6 (2011) 2943.
34. F. Zhang, D.-D.Qi, and X.G Zhang, *Int. J. Electrochem. Sci.*, 11 (2016)189.
35. Y.I. Zhou, Z.B. Hu, C.H. Zhao, K.Y. Liu, and D.-G. Lin, *Int. J. Electrochem. Sci.*, 11 (2016) 6078.
36. H. Zhang, Y. Dai, H. Zhang, W. Wang, Q. Huang, Y. Chen, and L. Pu, *Int. J. Electrochem. Sci.*, 11 (2016) 6279.
37. Y. Li, S. Zhang, Q. Chen, and J. Jiang, *Int. J. Electrochem. Sci.* 10 (2015) 6199.
38. M. Aghazadeh, M. Hosseinifard, B. Sabour, and S. Dalvand, *Appl. Surf. Sci.* 287 (2013) 187.
39. P. Razmjoo, B. Sabour, S. Dalvand, M. Aghazadeh, and M.R. Ganjali, *J. Electrochem. Soc.* 161 (2014) D293.
40. M. Aghazadeh, *J. Appl. Electrochem.* 42 (2012) 89.
41. M. FátimaMontemor, S. Eugénio, N. Tuyen, R. P. Silva, T. M. Silva, and M. J. Carmezim, *Handbook of Nanoelectrochemistry* (2015) 1-27.
42. H.M. Shiri, and M. Aghazadeh, *J. Electrochem. Soc.* 159 (2012) E132.
43. R. Pavul Raj, P. Ragupath, and S. Mohan, *J. Mater. Chem. A*, 3 (2015) 24338.
44. M. Aghazadeh, A. Bahrami-Samani, D. Gharailou, M. Ghannadi Maragheh, M. R. Ganjali, and P. Norouzi, *J. Mater. Sci.: Mater. Electron.* 27 (2016) 11192
45. M. Aghazadeh, M. Ghannadi Maragheh, M.R. Ganjali, P. Norouzi, and F. Faridbod, *Appl. Surf. Sci.* 364 (2016) 141.
46. J. Duay, E. Gillette, J. Hu, and S. B. Lee, *Phys. Chem. Chem. Phys.*, 15 (2013) 7976.
47. M. Aghazadeh, H. Mohammad Shiri, and A. A. Malek Barmi, *Appl. Surf. Sci.* 273 (2013) 237.
48. M. Aghazadeh, A. A. Malek Barmi, and T. Yousefi, *J. Iran Chem. Soc.* 9 (2012) 225.
49. M. Aghazadeh, and S. Dalvand, *J. Electrochem. Soc.* 161 (2014) D18.
50. A.A. Malek Barmi, M. Aghazadeh, and H. Mohammad Shiri, *Chem. Phys. Lett.* 541 (2012) 65.
51. T. Nguyen, M. Boudard, M.J. Carmezim, and M.F. Montemor, *Electrochim. Acta* 202 (2016) 166.
52. J.B. Condon, *Surface Area and Porosity Determinations by Physisorption*, Elsevier Science, First edition (2016).
53. Y. Wang, Y. Lei, J. Li, L. Gu, H. Yuan, and D. Xiao, *ACS Appl. Mater. Interfaces* 6 (2014) 6739.
54. D.S. Dhawale, G.P. Mane, S. Joseph, S.N. Talapaneni, C. Anand, A. Mano, S.S. Aldeya, K.S. Lakhia, and A. Vinu, *RSC Adv.* 5 (2015) 13930.